BİTLİS EREN ÜNİVERSİTESİ
FEN BİLİMLERİ DERGİSİ

ISSN: 2147-3129 / e-ISSN: 2147-3188

Article Type : Research Article
Received : March 25, 2025
Revised : May 3, 2025
Accepted : May 13, 2025
DOI : 10.17798/bitlisfen.1665236

Year : 2025
Volume : 14
Issue : 2
Pages : 1204-1219

PROGRESSIVE COLLAPSE ANALYSIS OF REINFORCED CONCRETE BUILDING STRUCTURES

Julide YUZBASI [1]

[1] *Cukurova University, Engineering Faculty, Department of Civil Engineering, Adana, Türkiye, jyuzbasi@cu.edu.tr*

ABSTRACT

This study investigates the progressive collapse (PC) behavior of three reinforced concrete (RC) structure using the Applied Element Method (AEM), focusing on corner and intermediate edge column removal. The research evaluates AEM's effectiveness in capturing structural failure mechanisms and its reliability in progressive collapse analysis. A 3×3-bay RC frame with varying story heights (4, 7, and 10 stories) was analyzed in Extreme Loading for Structures (ELS) software. Six different scenarios were examined by varying the number of stories and the removed column locations. The numerical models incorporated TBEC 2018-compliant lap splice extensions, mesh refinement at plastic hinge locations, and slab adjustments. Two progressive collapse scenarios were considered: (1) sudden removal of a corner column and (2) removal of an intermediate edge column. The displacement response at the upper end of the removed section was monitored over 3 seconds, accounting for vibration damping. For this robust structural example, numerical results revealed that taller buildings exhibited greater transient and residual displacements, with the 10-story case reaching up to twice the displacement of the 4-story case. Moreover, intermediate edge column removal consistently led to higher displacement values than corner column removal, especially in taller structures. The results highlight the influence of column location and story height on collapse progression.

Keywords: Applied Element Method (AEM), Progressive Collapse (PC), Reinforced Concrete (RC), Solid mechanics, Collapse, Nonlinear Dynamic Analysis (NDA).

1 INTRODUCTION

Progressive collapse (PC) is a structural failure mechanism in which an initial local failure, triggered by an extreme event, propagates through the structure, ultimately leading to the disproportionate failure of a substantial portion or even the entire building [1]. Over the

years, numerous cases of progressive collapse have been documented worldwide, resulting from a range of extreme events, including gas explosions, bombings, fires, design and construction errors, severe earthquakes, tsunamis, improper usage, accidents, and excessive loading [1].

Notable examples include the collapse of Ronan Point in London (1968) [2] (Figure1), Capitan Arenas in Barcelona (1972), the U.S. Marine Barracks in Beirut (1983), Hotel New World in Singapore (1986), the A.P. Murrah Federal Building in Oklahoma City (1995) [2], the Sampoong Department Store in Seoul (1995) (Figure2), Khobar Towers in Saudi Arabia (1996) [2], the World Trade Center buildings in the U.S. (2001) [3], Windsor Tower in Spain (2005) [4], the Achimoto Melcom Shopping Centre in Accra (2012), and the Rana Plaza factory in Bangladesh (2013) [5].

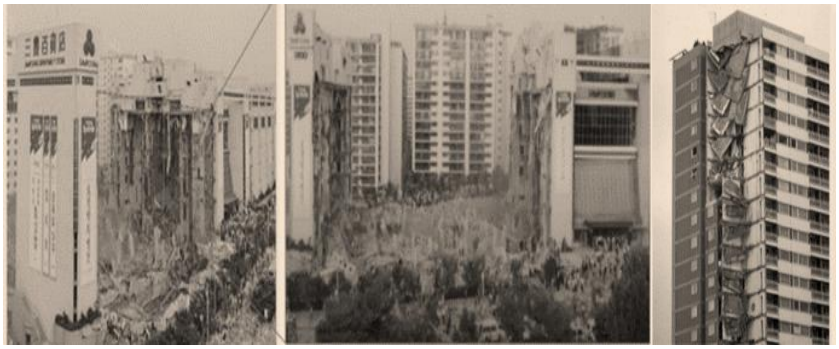


Figure1. Sampoong department store (Seoul, 1995) and Ronan Point (London, 1968).

On February 6, 2023, two devastating earthquakes with moment magnitudes of Mw 7.8 and Mw 7.6 struck nine hours apart, originating from the Pazarcık and Elbistan districts of Kahramanmaraş, Türkiye. These events caused widespread destruction across both urban and rural regions, significantly affecting the seismic performance of reinforced concrete (RC) and masonry structures. Various reconnaissance studies have since documented the extent of damage and contributed to understanding failure mechanisms. Avgın et al. [6] and Akar et al. [7] examined geotechnical and structural failures in Kahramanmaraş and Adıyaman, respectively, emphasizing the role of code compliance. Broader field surveys by Yuzbasi [8] and Dedeoğlu et al. [9] highlighted typical failure patterns and the importance of local soil conditions. Avcil et al. and Işık et al. reported widespread foundation and wall failures, highlighting the vulnerability of RC and masonry structures as well as Onat et al. [10–13], while Mete and Biyik [14] explored disaster management strategies using GIS-based tools. Çelik et al. [15] provided multidisciplinary assessments of mid-rise residential buildings, and recent studies have underscored the need for detailed performance evaluation to guide demolition or

retrofitting decisions [16–18]. Among the most frequently observed deficiencies were soft-story and weak-story mechanisms in low- to mid-rise buildings [19,20], which significantly contributed to the collapse patterns. Damage to cultural heritage and non-residential structures, including mosques and minarets, was also substantial in regions such as Malatya and Adıyaman [21–23]. These findings collectively underline the urgent need for both analytical and practical approaches to address seismic vulnerabilities in the built environment.

Unlike other studies, this work addresses the topic of progressive collapse and presents a research approach based on the Applied Element Method, which differs from conventional methods by utilizing 3D solid modeling where objects are interconnected through springs.

More recently, the partial collapse of the buildings in Türkiye, following the devastating 7.8 and 7.6 magnitude earthquakes in Kahramanmaraş on February 6, 2023, has further underscored the catastrophic consequences of progressive collapse (Figure2) [24].



Figure2. Alfred P. Murrah (USA, 1995); partially collapsed buildings (Turkiye, 2023).

2 MATERIAL AND METHOD

Applied Element Method (AEM) stands out as a hybrid approach that combines the strengths of both FEM and DEM. In AEM, structures are modeled as discrete elements connected by springs at nodal points, simulating both tensile and compressive behaviors (Figure3). These springs replicate the structural response to deformation, allowing the model to capture the initiation and progression of failure more effectively than traditional FEM. AEM is particularly valuable for simulating the collapse of structures, as it can model the separation and interaction of individual elements, a key feature in progressive collapse scenarios. In AEM, shear and normal springs are used to connect pairs of discrete elements at nodal points. These springs replicate the structural response to deformations, simulating both tensile and compressive behaviors. This method has been successfully applied in the modeling of full structural collapses, with many studies demonstrating its effectiveness [25–33]. Notably,

Grunwald et al. [34] compared FEM and AEM in their study, highlighting AEM's advantages in modeling structural collapse and its ability to account for local deformations and damage realistically.

In the context of the Applied Element Method (AEM), Normal Spring Stiffness (kn) and Shear Spring Stiffness (ks) play critical roles in defining how structural elements respond to axial and shear forces, respectively. Both normal and shear stiffnesses are used to define the interaction between discrete elements (such as beams, columns, or panels) that make up a structure. While normal stiffness primarily handles axial loads, shear stiffness is essential for simulating lateral deformations, helping to capture complex behaviors like sliding and buckling of structural members under extreme conditions [35-37]. In AEM, it primarily represents the stiffness of connections between elements that resist compressive or tensile forces along the axis of the element. The normal stiffness is crucial for accurately simulating the interaction between connected elements under axial loading conditions [36, 37].

The Normal Spring Stiffness is defined by the following Eq. 1:

$$k_n = \frac{E.\mathrm{A}}{d} \tag{1}$$

where:

E is the Young's modulus of the material, representing its resistance to axial deformation. A is the cross-sectional area of the spring connection, indicating how much force the element can carry per unit of deformation and d is the distance between connected nodes, reflecting the spatial relationship between points in the model.

In AEM, Shear Spring Stiffness is used to model the shear response of the connections between elements. This parameter is particularly important for simulating the behavior of structures under shear forces, which are common in earthquake and blast simulations. Shear stiffness defines how the elements deform when subjected to transverse forces that cause sliding between adjacent parts.

The Shear Spring stiffness is given by the formula Eq. 2:

$$k_s = \frac{G.A_s}{d} \tag{2}$$

where:

G is the shear modulus of the material, which describes its ability to resist shear deformation. As is the effective shear area of the connection, representing the region where shear forces are transferred and d is the distance between connected nodes, similar to the normal spring stiffness. This parameter is particularly important for simulating the behavior of structures under shear forces, which are common in earthquake and blast simulations. Shear stiffness defines how the elements deform when subjected to transverse forces that cause sliding between adjacent parts (Figure3).

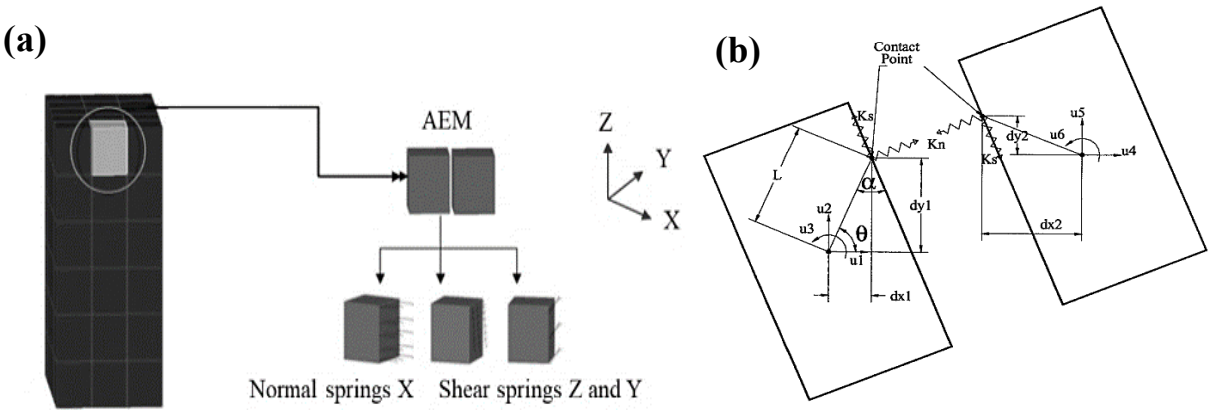


Figure3. AEM element model(a) and types of springs(b).

The stiffness matrix for a pair of springs (denoted as Ks positioned at coordinates (x, y, z) relative to the centroid of the first element is expressed by Equation1 and Equation2. This matrix represents the relationship between the applied forces and displacements at the connection point, capturing the behavior of the spring system under loading conditions. The stiffness of the springs, influenced by material properties and geometry, governs the system's deformation under external forces (Figure4).

$$K = \begin{bmatrix} k_n & 0 & 0 & 0 & k_n z & -k_n y \\ 0 & k_s & 0 & -k_s z & 0 & k_s x \\ 0 & 0 & k_s & k_s y & -k_s x & 0 \\ 0 & -k_s z & k_s y & k_s(y^2+z^2) & -k_s xy & -k_s xz \\ k_n z & 0 & -k_s x & -k_s yx & k_n z^2 + k_s x^2 & -k_n yz \\ -k_n y & k_s x & 0 & -k_s zx & -k_n zy & k_n y^2 + k_s x^2 \end{bmatrix}$$

Figure 4. AEM the stiffness matrix.

The forces needed to generate the configuration are represented by the components of the stiffness matrix, calculated by summing the contributions from all surrounding springs. As illustrated in Figure 8, the contribution of the contact spring to the degrees of freedom (DOFs) u1, u2, and u3 is equivalent to one-quarter of the element stiffness matrix. To form the global

stiffness matrix K, the individual contributions from each spring in the system are aggregated (Figure5). In the Applied Element Method (AEM), the stiffness matrix is essential for determining the structure's response to forces applied at discrete points, which correspond to connections between elements. These contributions reflect the stiffness of the individual springs that model the interactions between the elements [36, 37].

$$\begin{bmatrix} \sin^2(\theta+\alpha)K_n + \cos^2(\theta+\alpha)K_s & -K_n\sin(\theta+\alpha)\cos(\theta+\alpha) + K_s\,sin(\theta+\alpha)\,cos(\theta+\alpha) & K_s\,Lsin(\alpha)\,cos(\theta+\alpha) - sin(\theta+\alpha)\,K_n\,Lcos(\theta) \\ -K_n\sin(\theta+\alpha)\cos(\theta+\alpha) + K_s\,sin(\theta+\alpha)\,cos(\theta+\alpha) & \sin^2(\theta+\alpha)K_s + \cos^2(\theta+\alpha)K_n & \cos(\theta+\alpha)K_n\,Lcos(\theta) + \sin(\theta+\alpha)\,K_s\,Lsin(\theta) \\ \cos(\theta+\alpha)K_s\,Lsin(\alpha) - sin(\theta+\alpha)\,K_n\,Lcos(\alpha) & \cos(\theta+\alpha)K_n\,Lcos(\alpha) + \sin(\theta+\alpha)\,K_s\,Lsin(\theta) & L^2\,cos^2(\alpha)K_n + L^2\,sin^2(\alpha)K_s \end{bmatrix}$$

Figure5. One-quarter of the element stiffness matrix K [36, 37].

2.1 Main model

This study contributes to the field of progressive collapse analysis by systematically evaluating the structural response under sudden column loss conditions. For the main model, six analyses were conducted on reinforced concrete structures with 3×3 bays, each spanning 6 meters (Figure6). The building has a total span of 18.4 × 18.4 meters. The study considered three different building heights: 4, 7, and 10 stories. The structures utilized S420 steel reinforcement and C30 concrete. All columns had uniform cross-sectional dimensions of 40 cm × 40 cm, while beams measured 30 cm in width and 50 cm in depth. The slab thickness was 20 cm, with stirrups placed at 10 cm intervals for confinement. Lap splices were extended in accordance with TBEC 2018 provisions. A reinforcement ratio of 4% was applied to both columns and beams, with stirrups spaced at 10 cm intervals.

The models were meshed with careful consideration of potential plastic hinge locations, ensuring an appropriate distribution of finite elements. Beams were divided into 7 segments, columns into 44, and slabs into 49 segments, ensuring mesh compatibility at beam-column and beam-slab interfaces. In the slabs, the TSCF (Thin structure correction factor) factor was applied, and meshing was aligned with beam continuity for consistency. Each structural model underwent two distinct analyses. In the first scenario, a corner column at the ground floor was removed, and the displacement values at the upper end of the removed section were recorded

over a 3-second period. In the second scenario, an intermediate edge column was removed, and the resulting displacement at the removal location was examined. Figure 6 presents both the plan and elevation views of the building models used in the study. Subfigure (a) illustrates the plan view, while subfigure (b) shows the elevation views of the meshed 4-story, 7-story, and 10-story models, respectively. These visualizations provide insight into the geometric configuration and meshing strategy applied across varying building heights

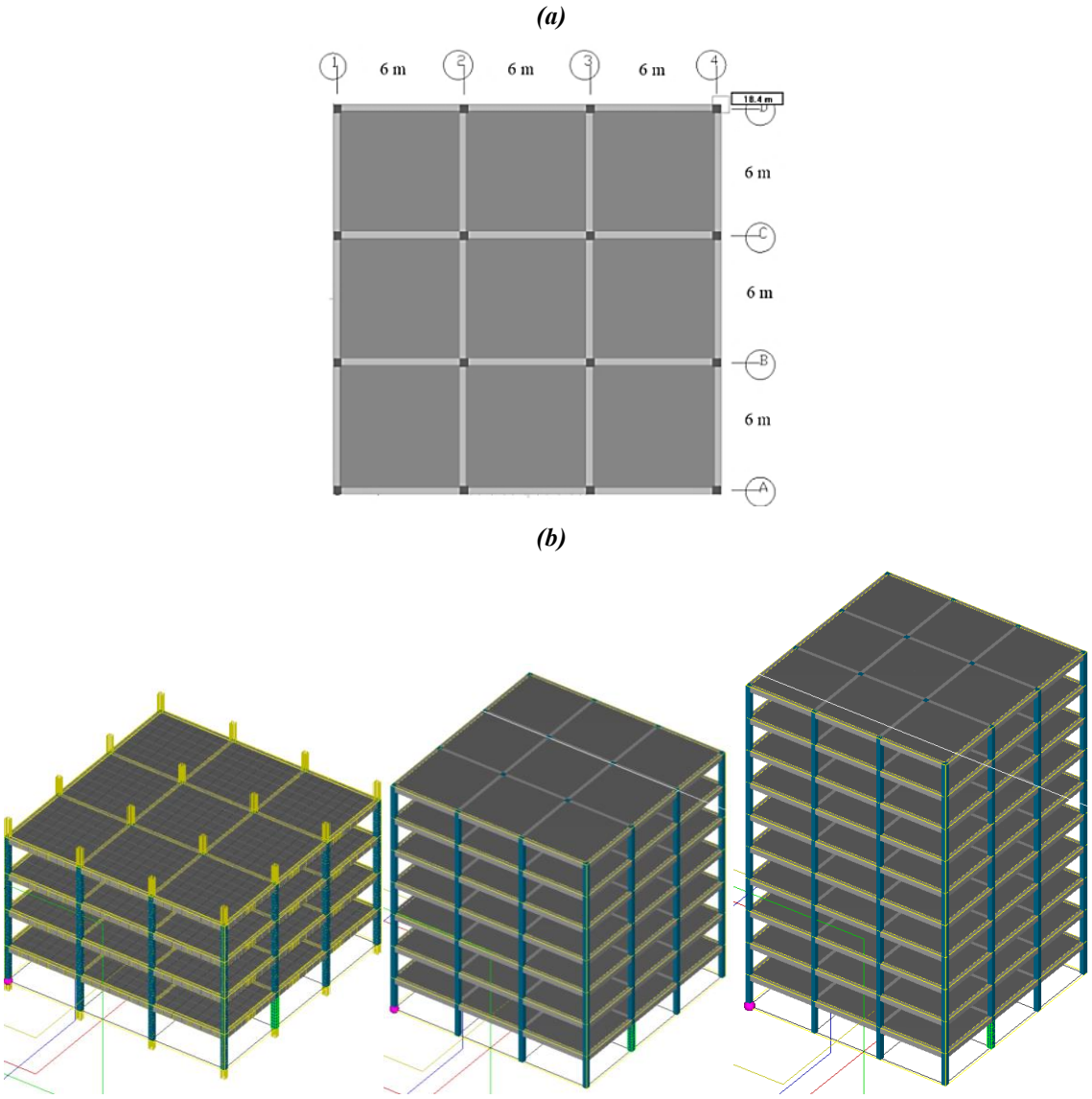


Figure6. Plan view (a) Elevational views of the 4-story meshed, 7-story, and 10-story model, respectively (b).

3 RESULTS AND DISCUSSION

The analysis was performed for three structural configurations with varying heights: 4-story, 7-story, and 10-story models. Each configuration was subjected to two column removal scenarios—corner column and intermediate edge column—to evaluate the structural response in terms of transient and residual vertical displacements. The displacement responses were derived from time-history analyses following column removal. The results for the 4-story, 7-story, and 10-story structures are presented sequentially in Figure 7–9, illustrating the outcomes for contours of corner column (a) and intermediate edge column removal (b) graphical results of corner column (c) and intermediate edge column removal (d), respectively.

Across all models and removal scenarios, the vertical displacement-time responses exhibit decaying oscillations characteristic of damped free vibrations. The 4-story model displays relatively higher-frequency, low-amplitude vibrations that dissipate more rapidly. As the number of stories increases, the vibration frequency decreases and the oscillations become more sustained, particularly in the 10-story model. The amplitude of the initial peak displacement also increases with building height, and the damping behavior appears less abrupt in taller structures. The plots consistently reflect a shift toward more pronounced dynamic effects as structural height increases, regardless of the removal location. The vibration characteristics reveal a trend of increased displacement amplitude and reduced damping as the number of stories increases. Shorter structures exhibit higher-frequency oscillations that decay more rapidly, whereas taller buildings display more sustained low-frequency vibrations. The corresponding stress distribution contours and displacement-time histories are presented in Figures. 7–9, where each column removal scenario is detailed graphically.

In the 4-story model (Figure7), the maximum transient vertical displacement recorded during corner column removal reached approximately -4.39 mm, with a residual displacement of -3.06 mm. Under the intermediate edge column removal scenario, the transient displacement increased slightly to -4.61 mm, and the residual displacement was measured as -3.49 mm.

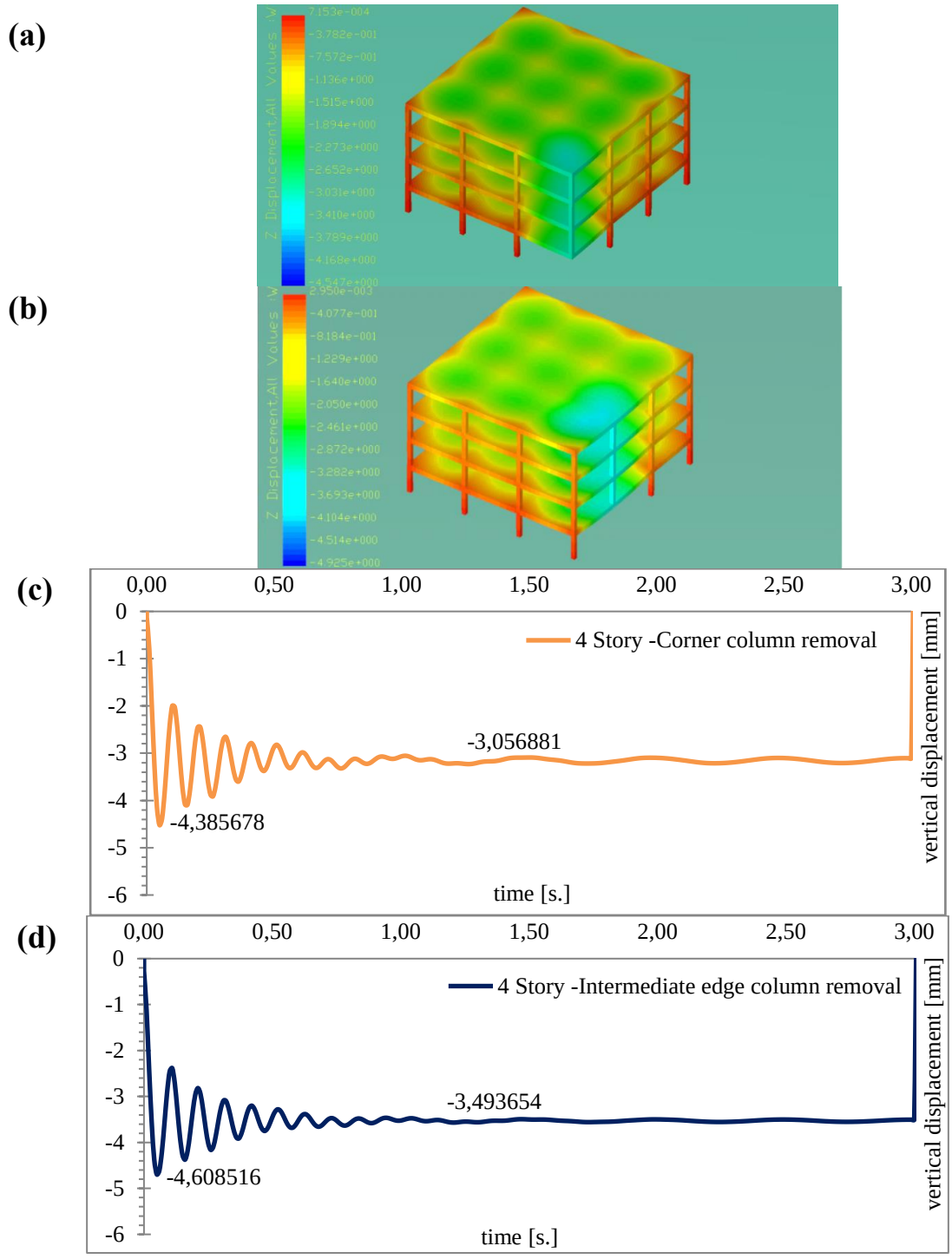


Figure7. 4-Story; Contours of corner column (a) and intermediate edge column removal (b) graphical results of corner column (c) and intermediate edge column removal (d)

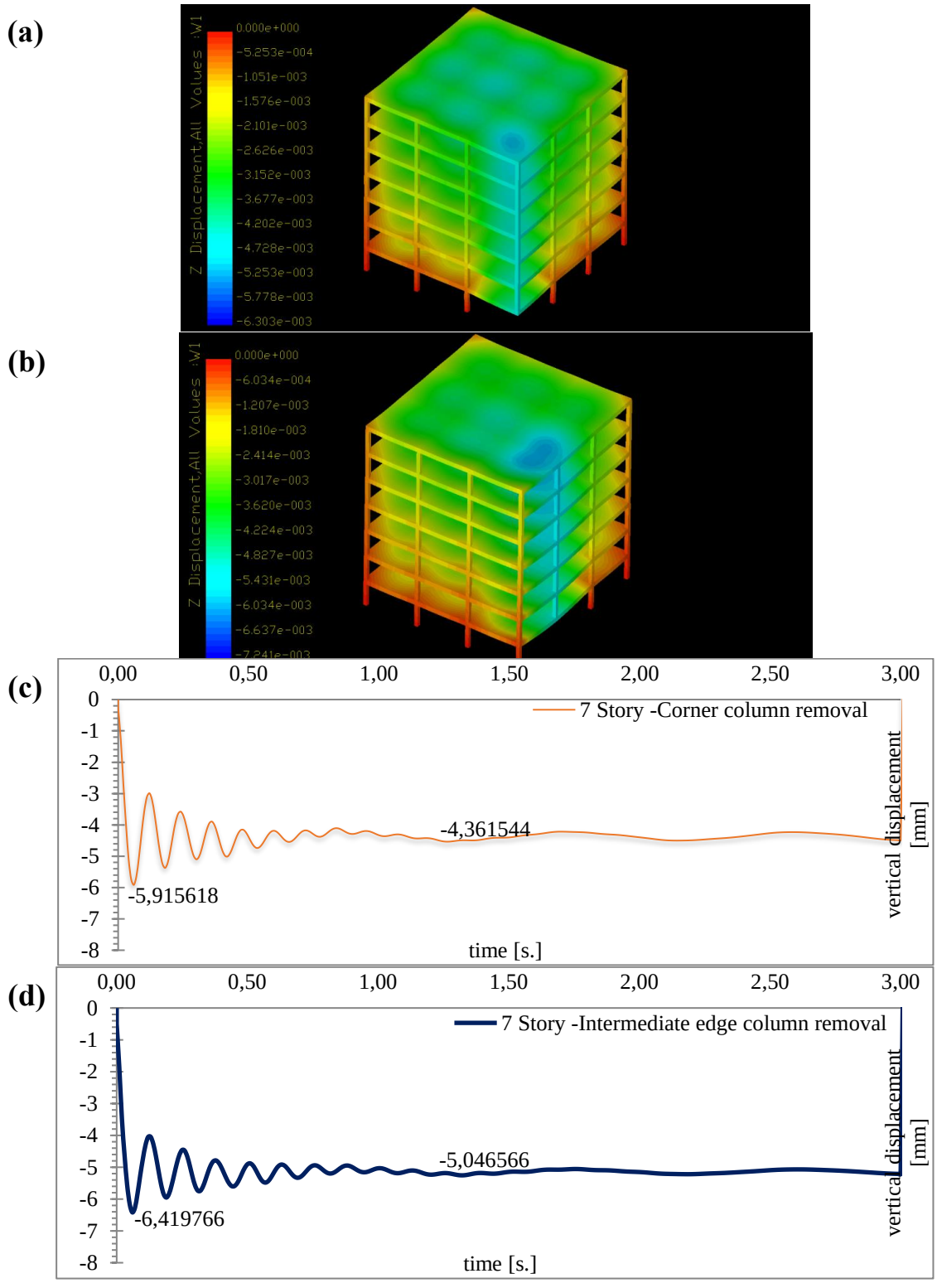


Figure8. 7-Story; Contours of corner column (a) and intermediate edge column removal (b) graphical results of corner column (c) and intermediate edge column removal (d)

For the 7-story building (Figure8), corner column removal resulted in a transient displacement of approximately -5.92 mm, while the residual displacement settled at -4.36 mm. In the case of intermediate edge column removal, the transient displacement reached -6.42 mm, and the residual displacement was -5.05 mm.

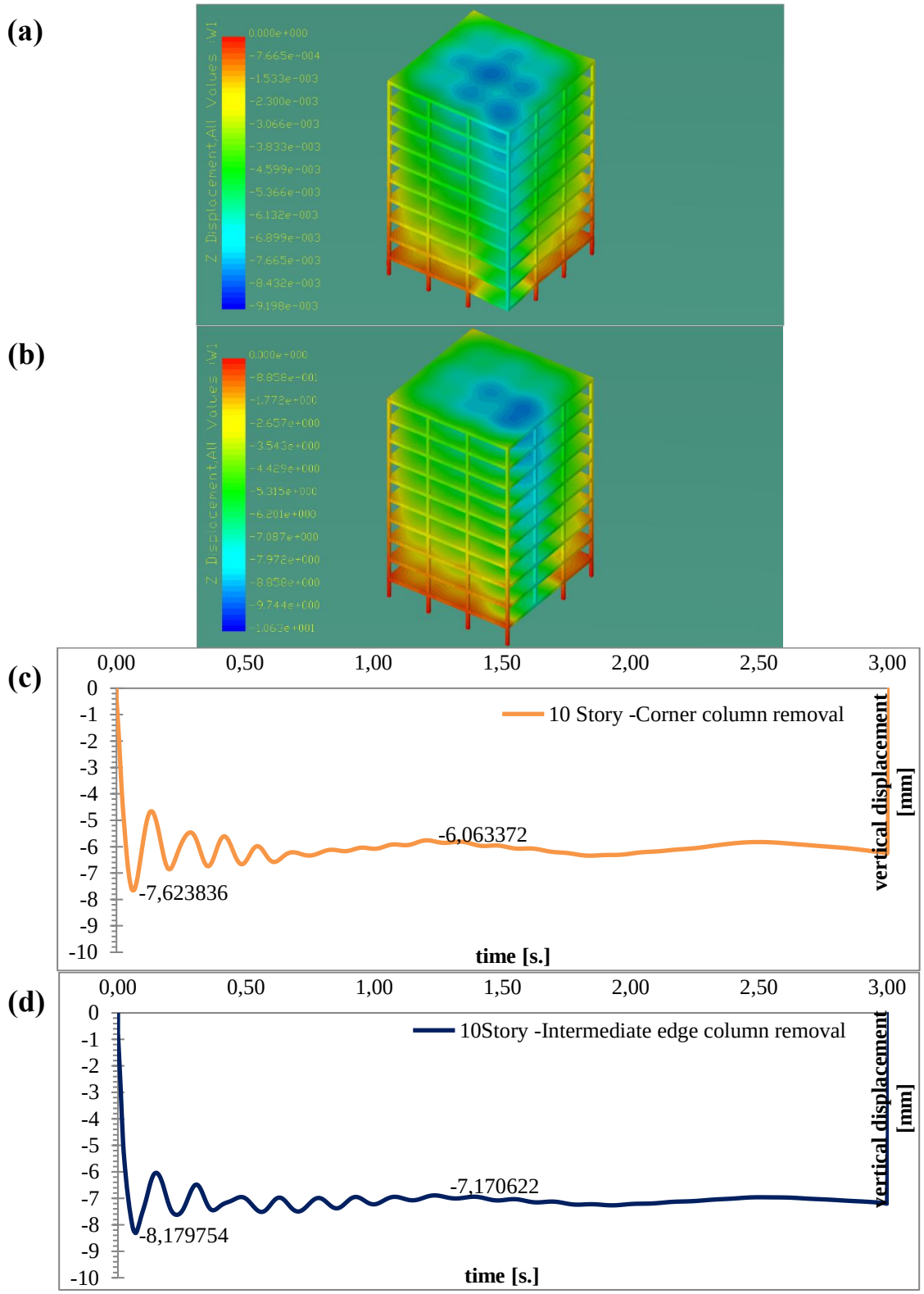


Figure9. 10-Story; Contours of corner column (a) and intermediate edge column removal (b) graphical results of corner column (c) and intermediate edge column removal (d)

Lastly, in the 10-story model (Figure9), the maximum transient vertical displacement under corner column removal was observed at -7.62 mm, with a corresponding residual displacement of -6.06 mm. For the intermediate edge column removal scenario, the transient displacement increased to -8.18 mm, and the residual displacement was recorded as -7.17 mm.

The numerical analysis of progressive collapse for reinforced concrete (RC) structures of varying story heights (4, 7, and 10 stories) reveals significant differences in structural response based on the location of column removal and the number of stories. The results are discussed in terms of maximum transient displacement and residual displacement.

Table 1. Transient and residual displacements for column removal scenarios.

Story Height	Column Removal	Max Transient Displacement (mm)	Residual Displacement (mm)
4 Stories	Corner Column	-4.39	-3.06
	Intermediate Edge Column	-4.61	-3.49
7 Stories	Corner Column	-5.92	-4.36
	Intermediate Edge Column	-6.42	-5.05
10 Stories	Corner Column	-7.62	-6.06
	Intermediate Edge Column	-8.18	-7.17

3.1 Effect of story height on displacement

The displacement results indicate that as the number of stories increases, both the maximum transient displacement and the residual displacement also increase. This trend is observed in both corner column and intermediate edge column removal scenarios. The 4-story structure exhibited the smallest deformations, while the 10-story structure showed the largest deformations. This suggests that taller buildings are more susceptible to larger displacement magnitudes due to increased mass and inertia, which influence the dynamic response of the structure.

3.2 Comparison of corner and intermediate edge column removal

For all cases, the removal of an intermediate edge column resulted in slightly larger displacement values compared to the removal of a corner column. This difference is more pronounced in taller structures. For example, in the 10-story case, the maximum transient displacement reached -8.18 mm for the intermediate edge column removal, whereas the corner

column removal resulted in -7.62 mm. Similarly, residual displacement values followed this pattern, with the intermediate edge column removal showing a higher value (-7.17 mm) than the corner column removal (-6.06 mm). The increased displacement in the intermediate edge column removal scenario may be attributed to the redistribution of loads and the greater dependency on adjacent structural elements.

3.3 Influence of column location on progressive collapse

The results confirm that column location plays a crucial role in progressive collapse behavior. The removal of a corner column, despite showing slightly lower displacement values compared to the intermediate edge column, still leads to significant structural instability. However, the intermediate edge column removal scenario tends to generate more severe progressive collapse effects due to the loss of support in a central load path.

3.4 Structural performance and implications

The increasing displacement values with higher story counts highlight the necessity of considering dynamic amplification effects when evaluating progressive collapse resistance in tall structures. Additionally, the observed differences between corner and intermediate edge column removal emphasize the importance of designing redundancy and alternative load paths in structural systems to mitigate collapse propagation.

Overall, these findings demonstrate the effectiveness of the Applied Element Method (AEM) in capturing structural failure mechanisms and provide critical insights into the behavior of RC buildings under progressive collapse scenarios. The results suggest that engineers should implement improved detailing strategies, such as enhanced reinforcement continuity and robust connection designs, to enhance structural resilience against sudden column loss events.

4 CONCLUSION AND SUGGESTIONS

This study investigated the progressive collapse behavior of a reinforced concrete (RC) frame under different column removal scenarios using the Applied Element Method (AEM). The results demonstrated that both transient and residual displacements increase with building height, indicating greater susceptibility to collapse in taller structures. Additionally, intermediate edge column removal led to slightly higher residual displacements compared to corner column removal, suggesting a greater redistribution of forces in these cases.

To enhance structural resilience against progressive collapse, it is recommended to improve detailing at critical connections, particularly in taller buildings. Incorporating redundancy through alternative load paths and reinforcing key structural elements can mitigate failure risks. Further studies should consider varying material properties, different loading conditions, and alternative strengthening techniques to develop more robust collapse-resistant design strategies [38,39]. As an additional analysis approach, future studies may explore gradually reducing the lateral stiffness of selected columns in earthquake-prone regions. Given the limitation of this study being confined to a single frame system layout, future research should consider alternative plan geometries and structural configurations, including systems incorporating shear walls and infill walls, to provide a more comprehensive understanding of structural behavior under varying conditions.

Acknowledgements

Gratitude is expressed to ASI for providing ELS.

Statement of Research and Publication Ethics

The study is complied with research and publication ethics.

Artificial Intelligence (AI) Contribution Statement

This manuscript was entirely written, edited, analyzed, and prepared without the assistance of any artificial intelligence (AI) tools. All content, including text, data analysis, and figures, was solely generated by the authors.

REFERENCES

[1] B. R. Ellingwood, R. Smilowitz, D. O. Dusenberry, D. Duthinh, H. S. Lew, and N. J. Carino, “Best practices for reducing the potential for progressive collapse in buildings,” 2007. [Online]. Available: https://tsapps.nist.gov/publication/get_pdf.cfm?pub_id=860696

[2] J. X. Lu, H. Wu, and Q. Fang, “Progressive collapse of Murrah Federal Building: Revisited,” *J. Build. Eng.*, vol. 57, p. 104939, 2022, doi: 10.1016/j.jobe.2022.104939.

[3] N. NCSTAR, “Final report on the collapse of the World Trade Center Towers,” *National Institute Standard Technology*, Gaithersburg, MD, 2005. [Online]. Available: https://nvlpubs.nist.gov/nistpubs/Legacy/NCSTAR/ncstar1.pdf

[4] J. Quiter, “Guidelines for designing fire safety in very tall buildings,” *Public Review Draft*, 2012.

[5] L. A. Bredean and M. D. Botez, “The influence of beams design and the slabs effect on the progressive collapse resisting mechanisms development for RC framed structures,” *Engineering Failure Analysis*, vol. 91, pp. 527–542, 2018, doi: 10.1016/j.engfailanal.2018.04.052.

[6] S. Avğın, M. M. Köse, and A. Özbek, "Damage assessment of structural and geotechnical damages in Kahramanmaraş during the February 6, 2023 earthquakes," *Eng. Sci. Technol. Int. J.*, vol. 57, p. 101811, 2024, doi: 10.1016/j.jestch.2024.101811.

[7] F. Akar, E. Işık, F. Avcil, A. Büyüksaraç, E. Arkan, and R. İzol, "Geotechnical and structural damages caused by the 2023 Kahramanmaraş earthquakes in Gölbaşı (Adıyaman)," *Appl. Sci.*, vol. 14, no. 5, p. 2165, 2024.

[8] J. Yuzbasi, "Post-earthquake damage assessment: Field observations and recent developments with recommendations from the Kahramanmaraş earthquakes in Turkiye on February 6th, 2023 (Pazarcık M7.8 and Elbistan M7.6)," *J. Earthq. Eng.*, pp. 1–26, 2024, doi: 10.1080/13632469.2024.2353864.

[9] I. O. Dedeoglu, M. Yetkin, G. Tunc, and O. E. Ozbulut, "Evaluating earthquake-induced damage in Dogansehir, Malatya after 2023 Kahramanmaras earthquake sequence: Geotechnical and structural perspectives," *J. Build. Eng.*, p. 112266, 2025, doi: 10.1016/j.jobe.2025.112266.

[10] F. Avcil *et al.*, "Effects of the February 6, 2023, Kahramanmaraş earthquake on structures in Kahramanmaraş city," *Natural Hazards*, vol. 120, no. 3, pp. 2953–2991, 2024.

[11] E. Işık *et al.*, "Field reconnaissance and earthquake vulnerability of the RC buildings in Adıyaman during 2023 Turkiye earthquakes," *Appl. Sci.*, vol. 14, no. 7, p. 2860, 2024, doi: 10.3390/app14072860.

[12] E. Işık *et al.*, "Structural damages in masonry buildings in Adıyaman during the Kahramanmaraş (Turkiye) earthquakes (Mw 7.7 and Mw 7.6) on 06 February 2023," *Eng. Fail. Anal.*, vol. 151, p. 107405, 2023, doi: 10.1016/j.engfailanal.2023.107405.

[13] O. Onat *et al.*, "Seismic resistance and performance evaluation of masonry dwellings after the February 6, 2023, Kahramanmaraş earthquake sequence in Türkiye," *J. Earthq. Tsun.*, vol. 18, no. 4, p. 2450013, 2024, doi: 10.1142/S1793431124500131.

[14] M. O. Mete and M. Y. Biyik, "Disaster management with cloud-based geographic information systems: Site selection of landfill areas after Kahramanmaraş, Turkiye earthquake sequence," *Environ. Earth Sci.*, vol. 83, p. 358, 2024, doi: 10.1007/s12665-024-11674-3.

[15] O. C. Celik *et al.*, "Multidisciplinary reconnaissance investigation covering structural, geotechnical, and architectural based damage to mid-rise residential buildings following the February 6th, 2023 Kahramanmaraş, Turkiye earthquake doublets (Mw 7.8, Mw 7.6)," *Soil Dyn. Earthq. Eng.*, vol. 182, p. 108738, 2024, doi: 10.1016/j.soildyn.2024.108738.

[16] J. Yuzbasi, "Controlled demolition: Novel monitoring and experimental validation of blast-induced full-scale existing high-rise building implosion using numerical finite element simulations," *J. Civil Struct. Health Monit.*, pp. 1–24, 2024, doi: 10.1007/s13349-024-00849-y.

[17] J. Yuzbasi, "Experimental verification of full-scale silo structure demolition: Investigating successive column removal with finite element method and progressive collapse simulation through blast load," *Struct. Concr.*, vol. 25, no. 6, pp. 4408–4427, 2024, doi: 10.1002/suco.202400017.

[18] T. P. Doğan *et al.*, "Investigation of RC structure damages after February 6, 2023, Kahramanmaraş earthquake in the Hatay region," *Bull. Earthq. Eng.*, vol. 22, no. 10, pp. 5201–5229, 2024, doi: 10.1007/s10518-024-01965-2.

[19] H. Ulutaş, "Investigation of the causes of soft-storey and weak-storey formations in low-and mid-rise RC buildings in Turkiye," *Buildings*, vol. 14, no. 5, p. 1308, 2024, doi: 10.3390/buildings14051308.

[20] I. B. Karasin, "Comparative analysis of the 2023 Pazarcık and Elbistan earthquakes in Diyarbakır," *Buildings*, vol. 13, no. 10, p. 2474, 2023, doi: 10.3390/buildings13102474.

[21] İ. Kocaman, Ö. Mercimek, M. Gürbüz, Y. Erbaş, and Ö. Anıl, "The effect of Kahramanmaraş earthquakes on historical Malatya Yeni Mosque," *Eng. Fail. Anal.*, vol. 161, p. 108310, 2024, doi: 10.1016/j.engfailanal.2024.108310.

[22] E. Işık *et al.*, "Structural damage evaluation of mosques and minarets in Adıyaman due to the 06 February 2023 Kahramanmaraş earthquakes," *Eng. Fail. Anal.*, vol. 151, p. 107345, 2023.

[23] E. Işık, "Structural failures of adobe buildings during the February 2023 Kahramanmaraş (Turkiye) earthquakes," *Appl. Sci.*, vol. 13, no. 15, p. 8937, 2023.

[24] *StEER*, "2023 Mw 7.8 Kahramanmaras, Turkiye Earthquake Sequence Preliminary Virtual Reconnaissance Report (PVRR) Media Repository," pp. 97–98, 2023, doi: 10.17603/ds2-mm04-xq43.

[25] Y. Yu and X. Zhu, "Nonlinear dynamic collapse analysis of semi-rigid steel frames based on the finite particle method," *Engineering. Structures*, vol. 118, pp. 383–393, 2016, doi: 10.1016/j.engstruct.2016.03.063.

[26] F. Dinu, I. Marginean, and D. Dubina, "Experimental testing and numerical modelling of steel moment-frame connections under column loss," *Engineering. Structures*, vol. 151, pp. 861–878, 2017, doi: 10.1016/j.engstruct.2017.08.068.

[27] A. I. Zerin, A. Hosoda, H. Salem, and K. M. Amanat, "Seismic performance evaluation of masonry infilled reinforced concrete buildings utilizing verified masonry properties in applied element method," *ACT*, vol. 15, no. 6, pp. 227–243, 2017.

[28] C. Cismasiu, A. P. Ramos, I. D. Moldovan, D. F. Ferreira, and J. B. Filho, "Applied element method simulation of experimental failure modes in RC shear walls," *Comput. Concr.*, vol. 19, no. 4, pp. 365–374, 2017, doi: 10.12989/cac.2017.19.4.365.

[29] A. Elshaer, H. Mostafa, and H. Salem, "Progressive collapse assessment of multistory reinforced concrete structures subjected to seismic actions," *KSCE J. Civ. Eng*., vol. 21, no. 1, pp. 184–194, 2017.

[30] A. Garofano and P. Lestuzzi, "Seismic assessment of a historical masonry building in Switzerland: the 'Ancien Hôpital De Sion'," *Int. J. Archit. Heritage*, vol. 10, no. 8, pp. 975–992, 2016.

[31] H. Salem, S. Mohssen, Y. Nishikiori, and A. Hosoda, "Numerical collapse analysis of Tsuyagawa bridge damaged by Tohoku Tsunami," *J. Perform. Constr. Facil.,* vol. 30, no. 6, 2016.

[32] H.-S. Kim and H.-H. Wee, "Separation strain for progressive collapse analysis of reinforced concrete building using applied element method," *Adv. Struct. Eng*., vol. 19, no. 3, pp. 437–448, 2016.

[33] H. M. Salem and H. M. Helmy, "Numerical investigation of collapse of the Minnesota I-35W bridge," *Engineering Structures*, vol. 59, pp. 635–645, 2014, doi: 10.1016/j.engstruct.2013.11.022.

[34] C. Grunwald et al., "Reliability of collapse simulation–Comparing finite and applied element method at different levels," *Engineering Structures*, vol. 176, pp. 265–278, 2018, doi: 10.1016/j.engstruct.2018.08.068.

[35] J. Yuzbasi and H. M. Arslan, "Applied element method and finite element method for progressive collapse assessment: A comparative study on the influence of slab types, thicknesses, and damping via three incremental column removals," *Structures*, vol. 73, 2025, doi: 10.1016/j.istruc.2025.108358.

[36] K. Meguro, "Applied element method: a new efficient tool for design of structure considering its failure behaviour," *Urban Secur.*, vol. 18, 2001.

[37] K. Meguro and H. Tagel-Din, "Applied element method for structural analysis: theory and application for linear materials," *Struct. Eng./Earthq. Eng., JSCE*, vol. 17, no. 1, pp. 15, 2000.

[38] J. Yuzbasi and H.R. Yerli, "Betonarme Yapıların Deprem Etkisi Altında Performans Analizlerinin Yapılması ve Güçlendirilmesi," *Çukurova Univ. Mühendislik-Mimarlık Fakültesi Dergisi*, vol. 33, no. 2, pp. 273–286, 2018, doi: 10.21605/cukurovaummfd.510083.

[39] Işık E, Radu D, Harirchian E, Avcil F, Arkan E, Büyüksaraç A, Hadzima-Nyarko M. Failures in Reinforced-Concrete Columns and Proposals for Reinforcement Solutions: Insights from the 2023 Kahramanmaraş Earthquakes. *Buildings*. 2025; 15(9):1535. https://doi.org/10.3390/buildings15091535